Journal of Colloid and Interface Science 677 (2025) 781–789

Contents lists available at ScienceDirect

Journal of Colloid And Interface Science

journal homepage: www.elsevier.com/locate/jcis

Regular Article

Microtube self-assembly leads to conformational freezing point depression

Tatiana Yu. Komarova [a], Thomas Zinn [b,1], Theyencheri Narayanan [b], Andrei V. Petukhov [a], Jasper Landman [c,*]

[a] Van't Hoff Laboratory for Physical & Colloid Chemistry, Padualaan 8, Utrecht, 3584 CH, the Netherlands
[b] ESRF - The European Synchrotron, Grenoble, 38043, France
[c] Physics & Physical Chemistry of Foods, Wageningen University & Research, Bornse Weilanden 9, Wageningen, 6708 WG, the Netherlands

GRAPHICAL ABSTRACT

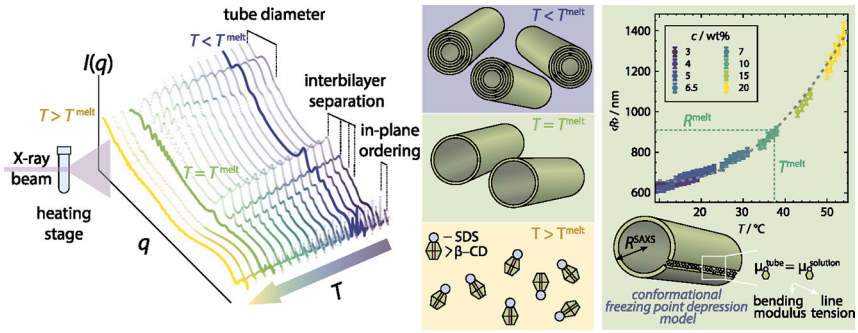

ARTICLE INFO

Dataset link: https://doi.org/10.15151/ESRF-ES-542848883

Dataset link: https://doi.org/10.15151/ESRF-ES-649492677

Keywords:
Hierarchichal self-assembly
Crystalline membrane
Membrane bending
Small-angle X-ray scattering (SAXS)

ABSTRACT

Hypothesis. Multi-walled tubular aggregates formed by hierarchical self-assembly of beta-cyclodextrin (β-CD) and sodium dodecylsulfate (SDS) hold a great potential as microcarriers. However, the underlying mechanism for this self-assembly is not well understood. To advance the application of these structures, it is essential to fine-tune the cavity size and comprehensively elucidate the energetic balance driving their formation: the bending modulus versus the microscopic line tension.

Experiments. We investigated temperature-induced changes in the hierarchical tubular aggregates using synchrotron small-angle X-ray scattering across a broad concentration range. Detailed analysis of the scattering patterns enabled us to determine the structural parameters of the microtubes and to construct a phase diagram of the system.

Findings. The microtubes grow from the outside in and melt from the inside out. We relate derived structural parameters to enthalpic changes driving the self-assembly process on the molecular level in terms of their bending modulus and microscopic line tension. We find that the conformation of the crystalline bilayer affects the saturation concentration, providing an example of a phenomenon we call conformational freezing point depression. Inspired by the colligative phenomenon of freezing point depression, well known from undergraduate physics, we model this system by including the membrane conformation, which can describe the energetics of this hierarchical system and give access to microscopic properties without free parameters.

* Corresponding author.
E-mail address: Jasper.Landman@wur.nl (J. Landman).
[1] Present address: Diamond Light Source Ltd, Harwell Science and Innovation Campus, Didcot, Oxfordshire OX11 0DE UK.

https://doi.org/10.1016/j.jcis.2024.08.003
Received 14 June 2024; Received in revised form 29 July 2024; Accepted 1 August 2024
Available online 6 August 2024

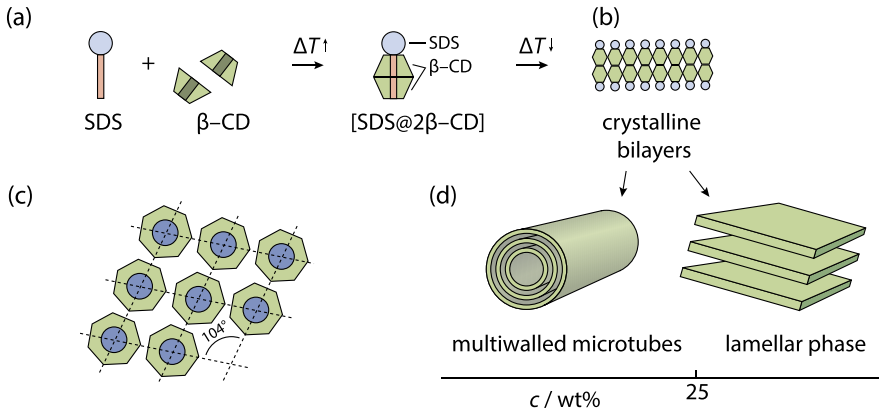

Fig. 1. Self-organization of β-CD and SDS into supramolecular aggregates. (**a**) The hydrophobic effect drives the formation of SDS@2β-CD complexes [12]. (**b**) Complexes assemble into bilayers, forming a two-dimensional rhombic crystalline membrane (**c**) via inter-cyclodextrin hydrogen bonding. The rhombic lattice, resulting from the 7-fold symmetry of the β-CD molecules, maintains a 104° angle to maximize inter-cyclodextrin hydrogen bonding [14].(**d**) Bilayer sheets assemble into superstructures depending on sample concentration [12]. Our study focuses on characterizing tubular aggregates.

1. Introduction

Self-assembly has long been recognized as a promising strategy for fabricating hierarchical, multiscale materials such as carbon nanotubes [1], peptide nanotubes [2,3], mesoscopic peptide-formed fibers [4–6], compositional tubule networks [7]. However, the application of self-assembly mechanisms has been limited by the need for precise tuning of the free energy landscape towards the desired function. To address this, carefully designed colloidal matter with DNA-encoded directed bonds [8], as well as hydrophobic [9] or magnetic [10] patches have been developed. Yet, in a hierarchical material, the free energy is contributed by not only its microscopic, molecular structure, but also its mesoscopic conformation. As such, it becomes challenging to predict how a system behaves given how the free energy landscape is dependent on that mesoscopic conformation. Here, we show that we can directly relate the mesoscopic structure of a hierarchical material to enthalpic changes occurring at both the molecular and conformational levels.

Recently, the self-assembling system of cyclodextrins and sodium dodecylsulfate has demonstrated a remarkable diversity in its mesoscale structures [11–15]. Depending on the concentrations of β-CD and SDS in aqueous solutions, lamellae, multi-walled microtubes as illustrated in Fig. 1, have been reported to form [12]. Along with these phases, this study proposed the existence of rhombic dodecahedra at lower concentrations. Yang et al. [14] characterized the internal structure of these supramolecular phases, highlighting their similarities to protein- and peptide-based aggregates. The tubular phase is particularly appealing as micro-carriers for controlled drug release [16], 1D artificial colloid confinement [17,18] and can serve as a model system for fundamental research on hierarchical self-assembly [19].

The self-assembly process of SDS and β-CD begins with the non-covalent host-guest interactions, yielding pocket-like inclusion complexes with 1:2 stoichiometry denoted by SDS@2β-CD [12,20,21]. These complexes subsequently arrange into a rhombic crystalline bilayer membrane with robust unit cell parameters, giving rise to diverse superstructures (Fig. 1C). Additionally, SDS@2β-CD aqueous solutions are easy to prepare, making them an ideal model system to study the effect of the mesostructural free energy landscape on self-assembly.

Multiple length scales involved in this system require structural analysis techniques that can probe them simultaneously. Synchrotron (ultra-)small-angle X-ray scattering is ideal for in situ structural analysis of such hierarchical systems. Advanced SAXS instrumentation achieves resolutions from the sub-nm range to a few microns, enabling the structural elucidation over many orders of magnitude [22]. As SAXS patterns can provide information on the shape and size of the constituents, this experimental technique is highly suitable for studying hierarchical microtube self-assembly. By analyzing SAXS profiles of samples at varying temperatures, we can identify features that enable the determination of the microtube diameter, as well as the inter- and intrabilayer periodicity. Through such analysis, we can gain insight into how the microtube structure on different hierarchical levels is influenced by changes in temperature and concentration.

In this article, we aim to explore the thermodynamic aspects of self-assembly of SDS@2β-CD microtubes. Solutions of varying SDS@2β-CD concentrations were examined at different temperatures using synchrotron SAXS. In our previous study, Ouhajji et al. [23] probed the structural properties of the system as a function of concentration at a fixed temperature. Then, Landman et al. [24] studied the kinetics of microtube formation after a temperature quench. Here, we perform a far wider detailed structural characterization of tubular aggregates, exploring temperature- and concentration-dependent microtube geometrical parameters. The obtained SAXS results enable direct access to nanoscopic energies involved in the self-assembly processes, as opposed to the bulk thermodynamic properties [25,26], revealing valuable insights into the mesoscopic microtube structure and constructing a partial microtube stability diagram.

In particular, we observe correlations between melting temperature, overall microtube diameter and SDS@2β-CD complex concentration. We model this relationship and find that the overal conformation of the complex crystalline bilayer affects the saturation concentration — providing an example of what can essentially be called conformational freezing point depression.

2. Materials and methods

2.1. Preparation of [SDS@2β-CD] microtube suspensions

β-CD (Sigma-Aldrich, 97%), SDS (Sigma-Aldrich, >99%) and Milli-Q water were weighed and mixed together in the desired amounts with a constant SDS to the β-CD 1:2 molar ratio. SDS was used to prepare samples as received. β-CD was preliminary dried to remove excess water [27]. A sample series with SDS@2β-CD concentrations ranging from 3 to 20 wt% was prepared. Mixtures were stirred and heated up to 70 °C (for concentrated samples of 15 wt% and up) or 50 °C (all other samples), until a turbid solution turned to a transparent liquid signifying the formation of SDS@2β-CD complexes. Hot solutions were kept for 48 hours at room temperature and transformed into viscous turbid gels indicating the tubular phase formation.

2.2. Temperature controlled SAXS experiment

All SAXS experiments have been performed at the Time-Resolved (Ultra)Small-Angle X-ray Scattering (TRUSAXS) beamline ID02, Euro-

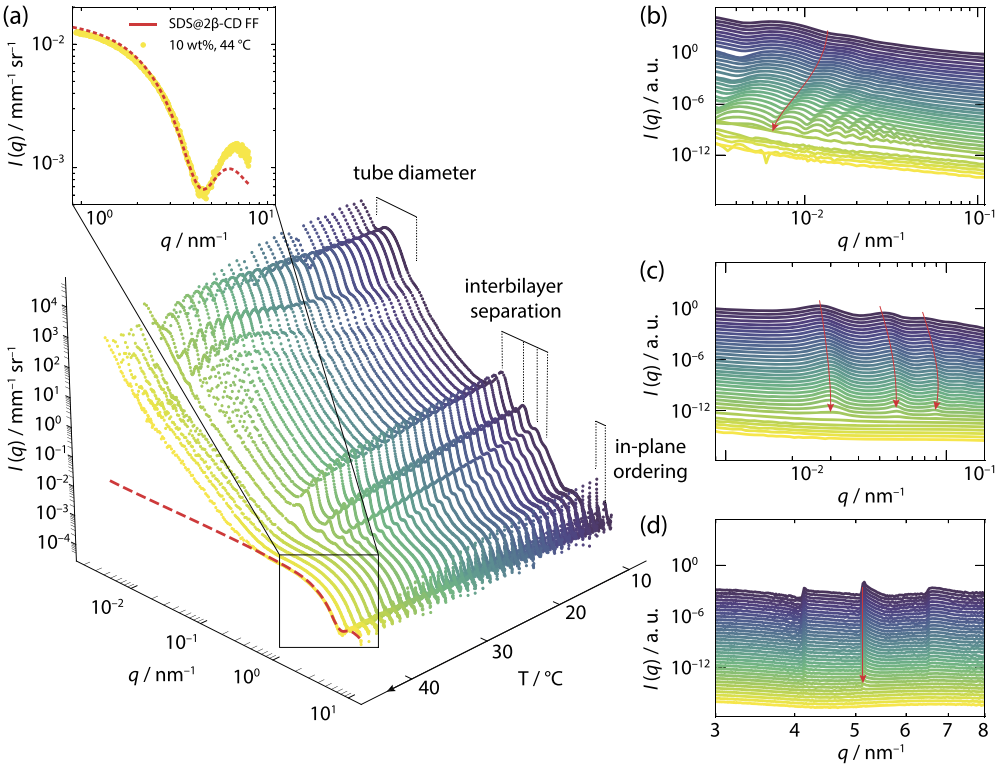

Fig. 2. Evolution of SAXS as a function of temperature for a 10 wt% sample. (**a**) Scattering intensity versus modulus of the scattering vector q with an arrow indicating the temperature change direction. The dashed red line represents the best fit of the experimental data modeled by the form factor of a SDS@2β-CD complex. Three main levels of the microtube organization are highlighted on the right: (**b**) oscillations related to the microtube radius at low q, (**c**) intermediate q region reveals regular wall spacing, (**d**) 2D crystal structure of the bilayer membrane at large q with the peak corresponding to the $[\bar{1}1]$ crystallographic direction in 2D rhombic lattice. Scattering curves in (**b**) – (**d**) are offset, and red arrows indicate specific scattering extremes. (For interpretation of the colors in the figure(s), the reader is referred to the web version of this article.)

pean Synchrotron Radiation Facility [28]. The incident X-ray wavelength was 1.01 Å. Scattering data were recorded using an Eiger2 4M (Dectris AG) hybrid pixel-array detector at two different sample-to-detector distance: 31 m for ultra-small angles (q_{min} = 0.002 nm^{-1}) and 1 m for larger angles (q_{max} = 8 nm^{-1}). These distances allow one to cover nominal sizes from 0.8 nm to 2.4 µm. Measured 2D SAXS patterns were normalized, regrouped and azimuthally averaged to obtain the 1D SAXS profiles as described elsewhere [28]. The background scattering curve was recorded at the same conditions as samples from a capillary filled with Milli-Q water.

To cover the full range of length scales in the system, from the microtube diameter down to the crystalline structure, the sample-to-detector distance has to be changed after the experiment is finished. Then, the scattering experiment is repeated under the same conditions with a freshly filled sample from the same vial, which was not modified during the first experiment. That provides identical conditions for all acquired scattering curves. Then, the recorded curves were merged to span all nominal length scales of interest.

Samples were loaded into sealed thin walled quartz capillaries with a diameter of 2 mm and were placed in a temperature controlled stage for multiple capillaries. To avoid the loading induced sample orientation, the capillaries were preliminary heated to a temperature at which all structural features corresponding to the tubular phase disappear (60 °C). This procedure ensured that the samples were brought to the same molten state. Then, the samples were gradually cooled down with a cooling rate of 0.2 °C/min and left for ten minutes at each set temperature to achieve equilibrium before recording a SAXS pattern. A downramp series was recorded in the temperature range of 70 °C-5 °C with a step of 1 °C. Afterward, a temperature upramp series was recorded using the same protocol, again allowing the system to equilibrate for 10 minutes before each measurement.

Results of the SAXS experiment were visualized and analyzed using the software SAXSutilities2 [29] in combination with custom Python scripts.

3. Results and discussion

3.1. Characterization of temperature-variation SAXS

Static upramp SAXS experiments were conducted at the Time-Resolved (Ultra-)Small-Angle X-ray Scattering (TRUSAXS) beamline ID02, European Synchrotron Radiation Facility [28] on samples of varying concentrations to investigate the temperature range encompassing microtube melting temperature. Data are available from ESRF [30], and extensive details of the experimental setup and analysis are thoroughly described in the supplementary materials.

Fig. 2 depicts 1D SAXS measurements of a 10 weight % (10 wt%) sample: curves display the sample scattering intensity $I(q)$ as a function of the modulus of scattering vector q for different temperatures T. Here, the magnitude of q relates to the angle of a scattered photon with respect to the incident beam, 2θ, as $q = 4\pi \sin\theta/\lambda$ with λ the wavelength of the incident x-rays. The 3D diagram illustrates temperature-induced sample restructuring across spatial length scales from 2.6×10^{-3} nm^{-1} to 8 nm^{-1}, which nominally corresponds to a real-space range of 0.8 nm to 2.4 µm.

Focusing on a specific range of q allows for the quantitative analysis of structural changes in the sample. The low q oscillations observed in Fig. 2B reveal the typical diameter of the microtubes. At low temperatures, these undulations are wide and shallow, indicating the presence of polydisperse and densely packed microtubes. As the temperature increases, higher order oscillations appear, signifying the microtubes becoming more uniform in their size. The shift in the minima to lower q values indicates an increase in the mean microtube diameter.

The results describe a melting trajectory where at lower temperature, the innermost microtubes melt while the larger microtubes remain. Through the melting trajectory, more and more of the inner microtubes melt until finally only a system of highly monodisperse, single-walled microtubes exists. The melting process essentially follows the reverse process of what we described in our earlier work [24]. The behavior shows some similarities to melting trajectories found in liquid crystal systems, where at low temperatures highly strained structures and long ranged order is lost, while some local orientational ordering is retained until higher temperatures. [31]

The sudden disappearance of numerous low q oscillations, coupled with a significant decrease of $I(q)$ at higher temperatures, points towards the disintegration of the microtubes into separate complexes. Beyond the melting point, oscillations in this q region are replaced by a power law decay ($\approx q^{-2}$), and the intensity at $q < 0.1\,\mathrm{nm}^{-1}$ drops dramatically. A similar behavior has been observed in the work [24] and is likely due to a residual amount of flat objects, potentially consisting of fragments of membranes.

At even higher temperatures, the recorded scattering patterns remain unchanged without many of scattering features. These scattering curves do not have any specific fingerprints except for a minimum at $\approx 4.5\,\mathrm{nm}^{-1}$ coming from the form-factor of the individual SDS@2β-CD complexes. At larger q values, the scattering curve can be fitted with a theoretical form factor of a SDS@2β-CD complex. The dashed red line in Fig. 2 shows the best fit result for the experimental data taken at 44 °C, which was obtained using molecular dynamics simulations that have been thoroughly described in previous studies [32,33].

Descending to the lower level of the microtube hierarchical self-assembly depicted in Fig. 2C, it is evident that pseudo-Bragg peaks are present in the microtube scattering patterns. These peaks refer to the specific distance d between walls inside a multi-walled tube that can be expressed by Bragg equation:

$$2\langle d\rangle \sin\theta = n\lambda, \tag{1}$$

where 2θ is the scattering angle, $\langle d\rangle$ - interbilayer separation between microtube walls, and n is an integer.

Higher harmonics with $n > 1$ of the repeat distance of the microtube layers can be observed at higher q values, as shown in Fig. 2C. With an increase in temperature, the lamellar peaks shift insignificantly to higher q values, indicating wall convergence. As the melting temperature is approached, the peak position shifts to lower q values and its intensity gradually decreases. According to Ref. [24], the inner layers of the multilayered tubes are less energetically stable due to the higher bending energy of the crystalline membrane they consist of, which leads to their melting at lower temperatures compared to the outer layers. This results in a drop in the lamellar peak intensity and, ultimately, its disappearance. The melting of the microtubes can also be observed in polarized light optical microscopy images taken from a sample at different temperatures, as shown in the supplementary materials. The gradual disintegration of the inner cylinders is accompanied by the release of pocket-like SDS@2β-CD complexes into the solution.

The highest q values in Fig. 2D provide insight into the internal crystalline structure of the microtubes. Previous studies, such as the work [14], have indicated that the microtubes are comprised of a crystalline bilayer membrane in which SDS@2β-CD complexes are arranged in a 2D rhombic lattice that optimizes the positioning of hydrogen bonds between the seven-fold symmetric cyclodextrins. The temperature-dependent behavior of three tooth-shaped peaks, corresponding to the [10], [$\bar{1}$1], and [11] in-plane crystallographic directions, is presented in Fig. 2D. The peak positions and, hence, rhombic unit cell parameters remain constant throughout the heating process. However, the peak intensities gradually decrease with increasing temperature and ultimately disappear around the melting temperature, indicating the absence of crystalline material in the observed volume.

The SAXS profiles obtained in this study enable both qualitative tracking of temperature-induced sample evolution and quantitative analysis of changes in various structural features of the microtubes, such as the outermost radius, number of walls, and inter-wall distance, as a function of temperature.

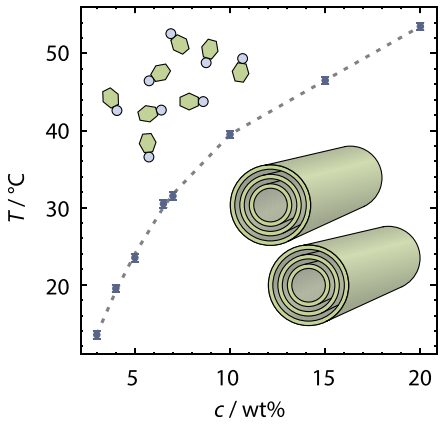

Fig. 3. Microtube melting point versus sample concentration. Circles represent transition points between microtubes and SDS@2β-CD complexes at various sample concentrations. The gray dashed line denotes the binodal.

3.2. Temperature-concentration phase space

The SAXS patterns for all concentrations show the same structural transformations: initially, polydisperse, densely populated multilayered tubes transform into more uniform objects, continuously breaking up into SDS@2β-CD single complexes. The absolute value of the transition point is dependent on the sample concentration. The melting temperature for each sample was determined using the partial Porod invariant, integrated within a specific q region, and the procedure is described in detail in the supplementary materials.

The existence of various phases in aqueous solutions of SDS@2β-CD complexes at room temperature has been reported previously in the study [14] In a more recent study, the phase behavior of pH-responsive surfactant-cyclodextrin complex mixtures was reported in Ref. [25]

By analyzing the upramp SAXS series, we have reconstructed a partial thermodynamic diagram in temperature-concentration coordinates, as shown in Fig. 3. At temperatures exceeding melting temperatures, no tubular aggregates were found, we exclusively observed SDS@2β-CD complexes. To the best of our knowledge, it is the first time that the full temperature-dependent behavior of our system has been demonstrated.

In general, an increase in sample concentration leads to a higher melting temperature. As previously observed in the temperature series of the 10 wt% sample (Fig. 2), only the form factor of single complexes is detected at temperatures exceeding the melting point. The same scattering curve evolution was observed for all concentrations investigated. Therefore, the dashed line in Fig. 3 separates the region of tubular phase existence and the region where only free single SDS@2β-CD complexes are present.

The restored transition point curve in Fig. 3 is located near the physiological temperature. The reversible transition between tubes and single complexes around the temperature of the human body could be exceptionally advantageous for controlled drug release. Due to the biocompatibility of β-cyclodextrin, an increasing number of studies [34,35], employ this cyclic oligosaccharide as a basic component to create nanocarriers and drug delivery systems.

3.3. Structural parameters

The scattering data were analyzed using a structural model of long concentric cylinders [36,37,23] and coexisting thin circular disks [38]. The model is described in detail in the supplementary materials. In Fig. 4A, B we show how the model can fit a scattering pattern at 10 wt%

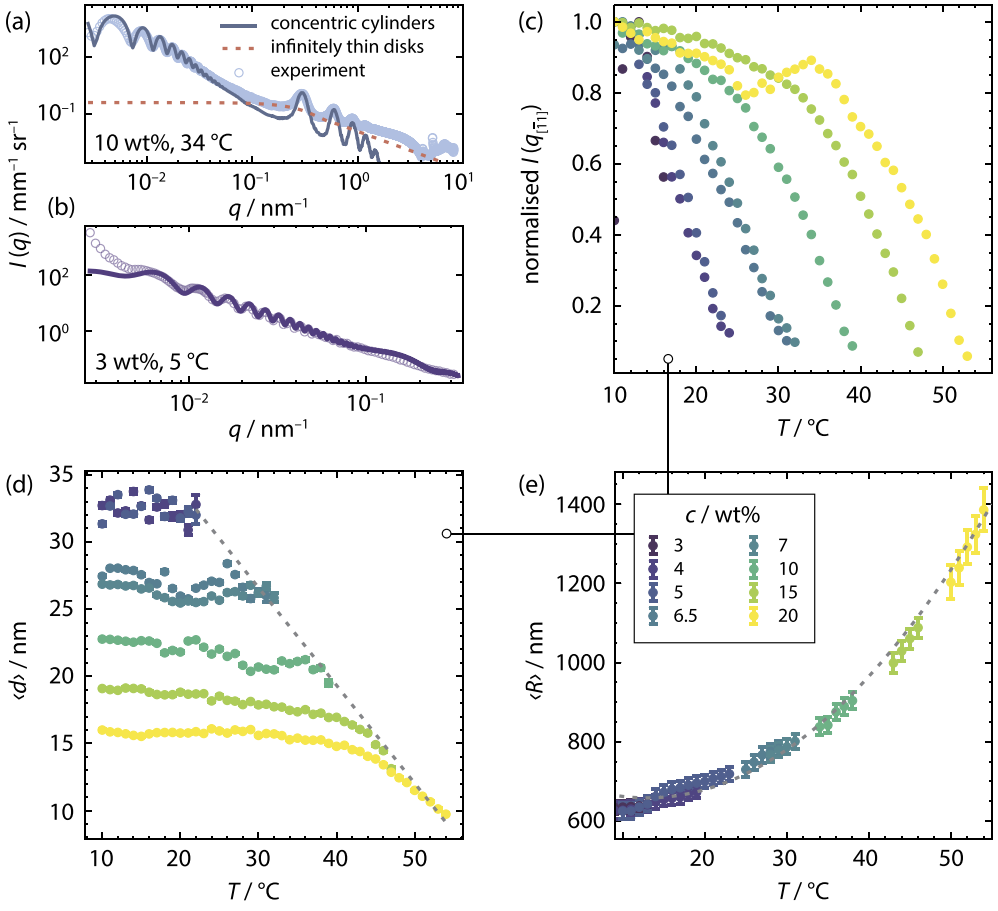

Fig. 4. Tracing the microtube parameters. (**a**) Azimuthally averaged scattering curve of the 10 wt% sample taken at 34 °C (blue) and the linear combination of scattering functions of concentric hollow cylinders (dark blue) and disks (red). (**b**) Experimental data taken from a 3 wt% sample recorded at 5 °C (circles) and the best fit obtained using the linear combination of concentric cylinders and disks (line). (**c**) Normalized scattering intensity of the crystalline membrane [$\bar{1}$1] peak as a function of the sample temperature. The apparent dip and recovery in the intensity of the 20 wt% sample is an artifact of the overlap of the [$\bar{1}$1] peak with the form factor minimum of the crystalline bilayer, as shown in Supplementary Fig. S6. (**d**) Interbilayer separation at different temperatures for various concentrations. For low concentrations, its value does not depend on the temperature and fluctuates around the average value. For higher concentrations, a certain decaying trend with the temperature increase is observed. (**e**) Microtube outermost radius for various concentrations. The values found from the fitting procedure follow a uniform temperature dependence. The gray dashed line corresponds to the parabolic fit line with empirical parameters of the best fit result.

and 3 wt% respectively. From the model we can quantitatively describe the scattering contributions of the multi-walled tubules, up to a scattering vector of $q = 1.8\,\mathrm{nm}^{-1}$. At higher q the sample scattering is governed by the crystalline organization of complexes within a bilayer, which is not taken into account in the model.

Fig. 4B demonstrates the ability of the proposed model to describe a SAXS curve taken from a 3 wt% sample at 5 °C. The fit is excellent at low to medium q, but a slight bump can be observed in the fit at around $0.2\,\mathrm{nm}^{-1}$ that has not been observed in the data. This bump is artificial and is likely a consequence of an inadequate polydispersity distribution in the disk size. A polyhedral capsid phase was found at $\lesssim 6$ wt% in cryo-EM micrographs [12]. We find no evidence for this phase in our experiments. SAXS patterns of samples recorded in this concentration regime all show the existence of the microtubular phase, as shown in the supplementary materials.

In Fig. 4C, we plotted the relative intensity of the most prominent intra-bilayer peak (in the [$\bar{1}$1] crystallographic direction) against temperature. Assuming that the tubular phase is the primary source of crystalline material in the system, this trend allows us to estimate the fraction of complexes that are released into the solution. For all concentrations, the intensity decay is the same, which suggests that the energetics of microtube disintegration is concentration-independent.

The distance between microtube walls can also be traced in the fitting procedure. As shown in Fig. 4D, the interbilayer separation is relatively constant for low concentrations within the available temperature range, whereas for higher concentrations, its value decreases with increasing temperature. In our previous work [24], we proposed an expression for this quantity

$$d = \sqrt{\frac{k_B T \sigma^2}{\rho_s} \frac{4\pi R^2}{\sqrt{3} a_0 \kappa c}}. \tag{2}$$

Here, k_B is the Boltzmann constant, σ represents the surface charge number density of the membrane, ρ_s is the salt number density, a_0 is the interfacial area occupied by a single SDS@2β-CD complex, κ is the bending modulus of the crystalline membrane, and c is the number density of SDS@2β-CD complexes.

The temperature term T in the numerator in eq. (2) intuitively suggests a positive correlation in the average distance with increasing temperature. However, highly concentrated samples demonstrate the opposite trend. The temperature driven decrease of d can be explained as an effect of the ionic strength increased by free SDS@2β-CD complexes. As the temperature increases, the inner layers of the microtubes disintegrate, providing additional macroions to the salt reservoir, screening the remaining electric double layer repulsions between the layers that remain.

Fig. 4E represents the outermost radius values obtained from the fitting procedure. Resulting values are temperature-dependent and exhibit

a uniform master curve that is independent of the sample concentration. A parabolic fit is shown as the gray dashed line, indicating that the microtube size increases with increasing temperature. We can infer from Fig. 4E that the microtube size is determined by the competition between energetic contributions that define the self-assembly path, which are independent of the sample concentration and change only with temperature.

3.4. Microtube melting model

In our earlier work we found that the mechanism is driven by the gain in free energy achieved by a crystalline bilayer of SDS@β-CD complexes when it closes to form a cylinder [24]. This happens at a definite size determined by optimizing the free energy gain per unit interface and the bending penalty. The outcome is a nucleation-dominated inward growth until a space-filling structure is formed.

In current temperature ramp experiments, we found that the innermost cylinders have the lowest melting temperatures. Essentially, when slowly increasing the temperature of a microtube system, the tubes melt from the inside out. This aligns with the idea that tightly curved inner cylinders gain less free energy upon closure due to increased bending energy.

Two key physical parameters influencing the melting behavior are the bond enthalpy of a complex being incorporated into the bilayer, and the bending modulus of that bilayer. Although direct access to these parameters is unavailable, we monitored key observables in the SAXS analysis of microtube melting: macroscopic complex concentration, melting temperature of the outermost cylinder, and outermost cylinder radius.

We propose a model here that is inspired by the classical derivation of the colligative property of freezing point depression — well known from undergraduate physics — although here it is not an added solute decreasing the chemical potential of the liquid state, but a conformational change increasing the chemical potential of the crystalline (bilayer) state. Deviations from the classical picture of colligative freezing point depression have previously been found in MD simulations of Lennard-Jones fluids in confinement [39]. The central assumption in the model proposed here is that the bond enthalpy of a complex being incorporated into a bilayer is temperature-dependent, but the bending modulus, at least to the first order, is constant. The crystalline nature of the membrane forming the tubular aggregates distinguishes it from soft matter composed of lipid bilayer membranes, as the latter is easily deformed, having a bending modulus typically not exceeding a few tens of k_BT [40,41]. While even minor temperature variations can significantly impact bilayer membranes, the bending modulus of SDS@β-CD microtubes is presumably notably higher and can be reasonably assumed to remain constant, irrespective of temperature changes. According to our previous study [24], the enthalpic contribution is expected to be significantly smaller, typically on the order of k_BT, as it characterizes the energy associated with the bonding interactions between cyclodextrin molecules [42,43].

The (Helmholtz) free energy of bending per unit interface of a sheet of material bent uniformly along one principal axis is given by

$$f_{\text{bend}} = \frac{\kappa}{2}\frac{1}{r^2}, \tag{3}$$

where κ is the elastic bending modulus of the bilayer [44] and r is the radius of the curvature. Here we have omitted the Gaussian curvature term, which is zero for all flat and cylindrical objects. Upon deforming a bilayer of width $2\pi r$ and length ℓ (assuming an approximately rectangular geometry) and closing the cylinder, the line tension along the length of the bilayer is removed. Per unit interface, the free energy gain of this process is given by

$$f_{\text{bond}} = -\frac{\tau}{2\pi}\frac{1}{r}, \tag{4}$$

where τ is the line tension, i.e. the free energy per unit length that arises from the unpaired bonds at the edge of the cylinder. In terms of microscopic quantities, the line tension τ scales with the typical bond energy through a lengthscale ℓ_0 that is on the order of the lattice parameter of the bilayer.

Combining the free energy of bending per unit interface and the free energy gain of closing the cylinder, and then setting the derivative with respect to r to 0, we find an optimum cylinder radius given by

$$r_0 = \frac{2\pi\kappa}{\tau}. \tag{5}$$

The optimal cylinder radius can be determined experimentally by analyzing SAXS patterns near the melting temperature. Eq. (5) relates κ and τ, connecting mesoscopic and molecular scales.

We now assume that at the melting point, there is an association equilibrium between a SDS@2β-CD complex incorporated into a tube, and a SDS@2β-CD complex floating free in solution. This assumption does not take into account any other larger self-assembled structures, such as the capsids found by Jiang et al. [12], but such a reservoir could be added to the equations in a straightforward way. In our experiments we found no evidence of such capsids at any temperature or concentration, as detailed in supporting section S1.3. This equilibrium is reminiscent of a surfactant solution that can self-assemble into micelles. As such, we can establish the equilibrium condition

$$\mu_A^{(\text{aq})} = \mu_A^{(\text{c})}, \tag{6}$$

with the superscripts now denoting the aggregation state of the complex. Assuming the ideal behavior of the solution, the chemical potential can be written as

$$\mu_A^{(\text{aq})} = \mu_A^{\circ(\text{aq})} + k_BT \log\frac{x_A}{x_A^\circ}, \tag{7}$$

where we have chosen an arbitrary concentration to act as the reference state for which μ_A° holds. Here, following our assumption of ideal behavior, x_A denotes the molar fraction of the complexes. The chemical potential of a complex inside the cylinder $\mu_A^{(\text{c})}$ can be seen as the reference chemical potential of a pure component, $\mu_A^\star$. We can identify $\Delta_r g_A \equiv \mu_A^\star - \mu_A^{\circ(\text{aq})}$ as the difference in reference chemical potentials as the standard molar Gibbs free energy of the reaction $\text{A(aq)} \rightleftharpoons \text{A(c)}$, which in turn can be split into an enthalpic and an entropic contribution.

$$\log\frac{x_A}{x_A^\circ} = -\frac{\Delta_r g_a}{k_BT} = \frac{\Delta_r h_A(T)}{k_BT} - \frac{\Delta_r s_A}{k_B}. \tag{8}$$

At this point, we take eq. (8) evaluated at the reference concentration x_A°,

$$\log\frac{x_A^\circ}{x_A^\circ} = 0 = \frac{\Delta_r h_A(T)}{k_BT^\circ} - \frac{\Delta_r s_A}{k_B}, \tag{9}$$

and subtract it from eq. (8) to cancel out the temperature-independent entropy terms. We are then left with

$$\log\frac{x_A}{x_A^\circ} = \frac{\Delta_r h_A(T)}{k_BT} - \frac{\Delta_r h_A(T^\circ)}{k_BT^\circ}. \tag{10}$$

Assuming that the enthalpic contribution $\Delta_r h_A$ in eq. (10) is equivalent to the bond energy gained from the complex incorporation into the bilayer, we say that

$$\Delta_r h_A(T) = -\frac{\ell_0\tau(T)}{2}, \tag{11}$$

where the factor 1/2 is introduced because the structure is a bilayer. This can be inserted into eq. (10) to yield

$$\log\frac{x_A}{x_A^\circ} = \frac{\ell_0\tau(T^\circ)}{2k_BT^\circ} - \frac{\ell_0\tau(T)}{2k_BT}. \tag{12}$$

While we do not have access to τ directly, we use the established relationship between the line tension τ and the experimentally accessible preferential radius R, where the bending modulus κ is considered

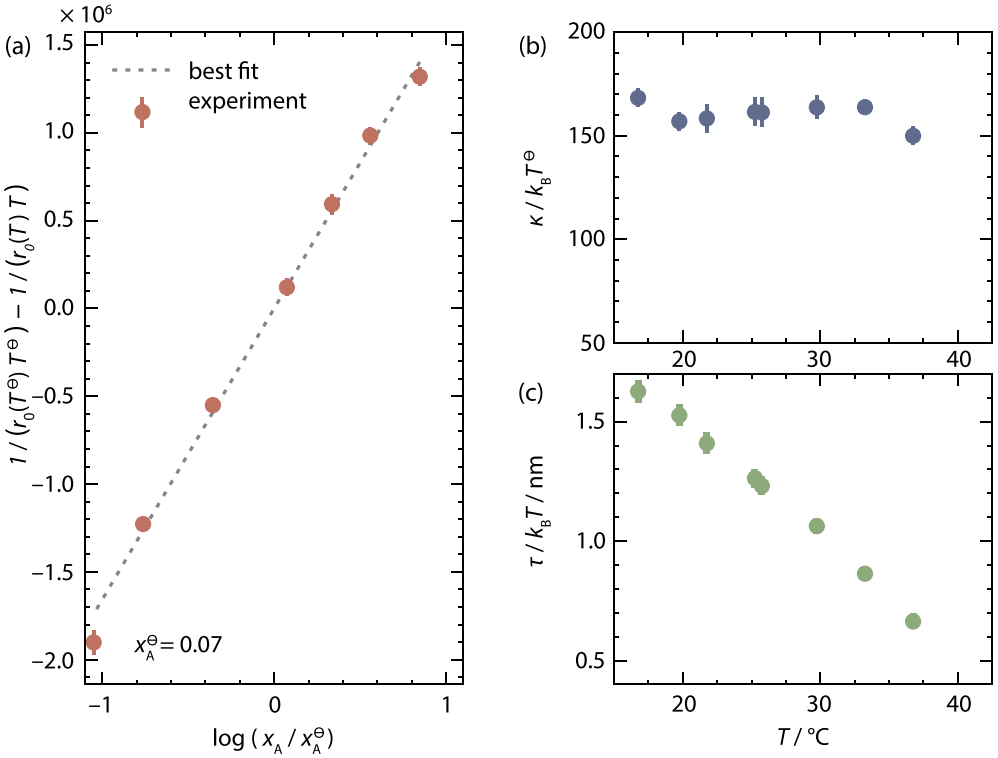

Fig. 5. Microtubule melting model applied to SAXS experimental data. (**a**) Experimental points and a linear trend following the developed model, eq. (13). A 7 wt% sample was used as a reference (x_A^*, T^*). (**b**) Bending modulus in k_BT units for differently chosen reference temperature T^* and (**c**) line tension values obtained from the model ($T^* = 298$ K).

constant across the entire temperature range. Additionally, the role of line tension in nucleation rate, as discovered in [24], provides an independent κ value, offering a parameter-free closure. From the nucleation rate at room temperature, a line tension is about 0.8 kT/nm.

We insert the relationship given by eq. (5) into the model, yielding

$$\log \frac{x_A}{x_A^*} = \frac{\ell_0 \pi \kappa}{r_0(T^*) k_B T^*} - \frac{\ell_0 \pi \kappa}{r_0(T) k_B T}. \tag{13}$$

We tested the derived expression against the experimentally determined outer radii as discussed above, where the melting temperature, the outermost radius value, and the sample concentration were considered the three main parameters necessary to access the energetics underlying tube formation. When plotting $[r_0(T^*)T^*]^{-1} - [r_0(T)T]^{-1}$ as a function of $\log x_A/x_A^*$, we obtain a straight line with slope $\ell_0\pi\kappa$, as can be seen in Fig. 5A for a chosen reference concentration of 7 wt%. The bending modulus can then be isolated directly from the proportionality constant. We verified the assumption of constant κ by choosing different sample concentrations as the reference state and obtained the corresponding slope and concurrent bending modulus. In Fig. 5B we show the fitted bending modulus as a function of the melting temperature of the chosen reference state. Indeed, we see that κ is independent of the selected reference state, validating our a posteriori assumption of a constant bending modulus. The ability to get this physical quantity from the SAXS experiment is extremely valuable: usually, more sophisticated methods are implemented [45].

Fig. 5C illustrates the line tension τ resulting from the fitting procedure. The model assumes that the line tension is essentially the enthalpy contribution: its value should lie around $\approx 1 k_BT\,\mathrm{nm}^{-1}$ [24], which is in line with current results. Moreover, we observe a decrease in τ with increasing temperature, consistent with earlier observations about the temperature dependence of hydrogen bonds which are the primary contribution to the line tension in this system [46] – as temperature rises, intensifying thermal fluctuations ultimately cause hydrogen bonds between β-cyclodextrins to break, with concomitant reduction of the line tension τ, and the microtubes disassemble.

As has been already mentioned, the SDS@2β-CD system shares some similarities with natural objects such as proteins and peptides [47–49]. The microtube membrane is rigid and crystalline, which is a significant difference from soft matter structures based on bilayers that are easily distorted and have a bending modulus that does not exceed tens of k_BT. Therefore, while slight temperature deviations can substantially affect soft matter structures based on bilayers, this is not the case for SDS@2β-CD tubes, whose bending modulus value is much larger.

The microtube melting model presented above, despite its simplicity and underlying assumptions, provides valuable insights into the energetic contributions crucial for microtube formation, directly derived from the SAXS experiment. The obtained micro- and macroscopic parameters enable us to manipulate the tube formation and vary the energetic contributions of different nature, providing guidance for designing and optimizing tube formation processes. Importantly, the model can be extended to other systems that operate at different length scales, providing a powerful tool for studying the disassembly and related energetic processes of such systems. For instance, similar models can be applied to SAXS data on peptide nanotubes or other amphiphilic systems forming nanotubes to track the conditions and geometrical parameters of their disassembly and relate them to the energy governing this process.

4. Conclusions

In this study, we have investigated the structural response of multi-walled tubular supramolecular aggregates formed in aqueous solutions of SDS and β-CD as a function of temperature and concentration by means of the SAXS technique. Furthermore, we propose a model, analogous to the freezing point depression phenomenon, locking in the driving forces of microtube self-assembly. Consequently we are able to find bending modulus and line tension values, derived solely on the results of a single SAXS experiment. The traditional approaches to obtain these variables are more resource-consuming [50].

Key parameters of tubular aggregates (e.g. outer radius, distance between shells) are of great potential to use these objects as microcarriers and artificial colloidal confinement. The use of SDS@β-CD microtubes as 1D confinement was previously demonstrated by studies [51,52]. Many ordered structures, such as linear chiral assemblies, zigzag, and zipper configurations of isotropic colloidal spheres, were synthesized with high yield employing their coassembly with microtubes [23,18]. We believe that the output of our study will significantly promote the coassembly of microtubes and colloidal particles to the next level and aid in the design of chiral materials, thanks to the demonstrated possibility to finely tune the size of the confinement depending on sample concentration or temperature.

While much has been known about the general morphology of multilamellar tubes in general (see e.g., [53–55]) and on this system in particular (see e.g., [13,14,23]), we go well beyond the morphological description alone. In a single experiment we are able to obtain experimentally hard to access parameters such as the line tension and bending modulus of a crystalline membrane, and show that these two parameters are key to the resulting superstructure. The slow assembly in a state of quasi-equilibrium essentially follows the same mechanism as for a rapid temperature quench [24] — that of inward growth by successive nucleation of new crystalline membranes constrained by existing outer cylinders. Similarly, when the temperature is slowly increased, the reverse process is observed: multilamellar microtubes melt from the inside out due to the fact that their tighter radius of curvature increases the chemical potential of the complexes.

Where the existing literature focuses on the appearance and morphology of the outermost cylinder [56], our work provides a key insight into the further self-assembly process: the mechanism by which microtubes self-assemble follows a growth process that is constrained by the morphology of an intermediate state. Indeed, based on the resulting line tension and bending moduli, the free energy per unit interface of a fully lamellar phase is lower than that of the microtubular phase, yet the microtubular phase is consistently found, regardless of whether the temperature is quenched quickly (see e.g., our previous work, [24] or slowly in quasi-equilibrium (as in this work). It is the strong stability of the single-walled microtubular state that essentially constrains the self-assembly process towards its eventual conclusion. This insight is not limited to this particular system at all, but depends simply on the existence of a strong line tension and rather stiff bending modulus, a very common feature in assemblies of crystalline membranes [57,25].

We believe that the presented results are of importance to a much broader range of systems. Similar analysis could be performed in a fairly straightforward fashion on other self-assembling systems of multilamellar microtubes, such as the 12-hydroxystearic acid / ethanolamine system (see e.g., [58]) or the self-assembly of bolaamphiphiles into single-walled nanotubes [59]. Indeed, in the latter work, the formation mechanism was demonstrated to follow the process of cylinder closure. Extending the analysis to more chemically distinct systems would require a different approach, but MD-simulations have already shown depressed freezing points for materials in strong confinement, such as in [60].

CRediT authorship contribution statement

Tatiana Yu. Komarova: Writing – original draft, Visualization, Methodology, Formal analysis, Data curation. **Thomas Zinn:** Writing – review & editing, Validation, Conceptualization. **Theyencheri Narayanan:** Writing – review & editing, Resources, Methodology, Conceptualization. **Andrei V. Petukhov:** Writing – review & editing, Validation, Supervision. **Jasper Landman:** Writing – review & editing, Supervision, Project administration, Formal analysis, Conceptualization.

Declaration of competing interest

The authors declare that they have no known competing financial interests or personal relationships that could have appeared to influence the work reported in this paper.

Data availability

Data is publicly available in ESRF repository with DOI https://doi.org/10.15151/ESRF-ES-542848883 and https://doi.org/10.15151/ESRF-ES-649492677

Acknowledgements

Bonny Kuipers is gratefully acknowledged for his help with the polarization microscopy setup. We acknowledge the European Synchrotron Radation Facility (ESRF) for provision of synchrotron radiation facilities, and the use of beamline ID02 for experiments SC-4987 and SC-5177, and for hosting TK for a traineeship.

Appendix A. Supplementary material

Supplementary material related to this article can be found online at https://doi.org/10.1016/j.jcis.2024.08.003.

References

[1] H. Shimoda, S.J. Oh, H.Z. Geng, R.J. Walker, X.B. Zhang, L.E. McNeil, O. Zhou, Self-assembly of carbon nanotubes, Adv. Mater. 14 (12) (2002) 899–901.
[2] I.W. Hamley, Peptide Nanotubes, Angew. Chem., Int. Ed. Engl. 53 (27) (2014) 6866–6881, https://doi.org/10.1002/anie.201310006, http://doi.wiley.com/10.1002/anie.201310006.
[3] C. Valéry, F. Artzner, M. Paternostre, Peptide nanotubes: molecular organisations, self-assembly mechanisms and applications, Soft Matter 7 (20) (2011) 9583, https://doi.org/10.1039/c1sm05698k, http://xlink.rsc.org/?DOI=c1sm05698k.
[4] A. Aggeli, I.A. Nyrkova, M. Bell, R. Harding, L. Carrick, T.C.B. Mcleish, A.N. Semenov, N. Boden, Hierarchical self-assembly of chiral rod-like molecules as a model for peptide-sheet tapes, ribbons, fibrils, and fibers, Proc. Natl. Acad. Sci. USA 98 (21) (2001) 11857–11862.
[5] L.E.R. O'leary, J.A. Fallas, E.L. Bakota, M.K. Kang, J.D. Hartgerink, Multi-hierarchical self-assembly of a collagen mimetic peptide from triple helix to nanofibre and hydrogel, Nat. Chem. 3 (10) (2011) 821–828.
[6] G.M. Whitesides, B. Grzybowski, Self-assembly at all scales, Science 295 (5564) (2002) 2418–2421.
[7] G.C. Wong, J.X. Tang, A. Lin, Y. Li, P.A. Janmey, C.R. Safinya, Hierarchical self-assembly of f-actin and cationic lipid complexes: stacked three-layer tubule networks, Science 288 (5473) (2000) 2035–2039.
[8] D. Nykypanchuk, M.M. Maye, D. Van Der Lelie, O. Gang, DNA-guided crystallization of colloidal nanoparticles, Nature 451 (7178) (2008) 549–552.
[9] Q. Chen, S.C. Bae, S. Granick, Directed self-assembly of a colloidal Kagome lattice, Nature 469 (7330) (2011) 381–384.
[10] S. Sacanna, L. Rossi, D.J. Pine, Magnetic click colloidal assembly, J. Am. Chem. Soc. 134 (14) (2012) 6112–6115.
[11] L. Jiang, Y. Peng, Y. Yan, M. Deng, Y. Wang, J. Huang, "Annular ring" microtubes formed by SDS@2β-CD complexes in aqueous solution, Soft Matter 6 (8) (2010) 1731–1736, https://doi.org/10.1039/b920608f.
[12] L. Jiang, Y. Peng, Y. Yan, J. Huang, Aqueous self-assembly of SDS@2β-CD complexes: lamellae and vesicles, Soft Matter 7 (2011) 1726–1731, https://doi.org/10.1039/c0sm00917b.
[13] L. Jiang, Y. Yan, J. Huang, Versatility of cyclodextrins in self-assembly systems of amphiphiles, Adv. Colloid Interface Sci. 169 (1) (2011) 13–25, https://doi.org/10.1016/j.cis.2011.07.002.
[14] S. Yang, Y. Yan, J. Huang, A.V. Petukhov, L.M.J. Kroon-Batenburg, M. Drechsler, C. Zhou, M. Tu, S. Granick, L. Jiang, Giant capsids from lattice self-assembly of cyclodextrin complexes, Nat. Commun. 8 (1585) 1–7, https://doi.org/10.1038/ncomms15856.
[15] L. d, S.S. Araújo, G. Lazzara, L. Chiappisi, Cyclodextrin/surfactant inclusion complexes: an integrated view of their thermodynamic and structural properties, Adv. Colloid Interface Sci. 289 (2021) 102375.
[16] K. Wang, H. Jin, Q. Song, J. Huo, J. Zhang, P. Li, Titanium dioxide nanotubes as drug carriers for infection control and osteogenesis of bone implants, Drug Deliv. Transl. Res. 11 (4) (2021) 1456–1474.
[17] L. Jiang, J.W.J. de Folter, J. Huang, A.P. Philipse, W.K. Kegel, A.V. Petukhov, Helical colloidal sphere structures through thermo-reversible co-assembly with molecular microtubes, Angew. Chem., Int. Ed. Engl. 52 (12) (2013) 3364–3368, https://doi.org/10.1002/anie.201209767, http://www.ncbi.nlm.nih.gov/pubmed/23441056.

[18] S. Ouhajji, B.G. Van Ravensteijn, C. Fernandez-Rico, K.S. Lacina, A.P. Philipse, A.V. Petukhov, Wet-chemical synthesis of chiral colloids, ACS Nano 12 (12) (2018) 12089–12095.
[19] H. Sun, Q. Luo, C. Hou, J. Liu, Nanostructures based on protein self-assembly: from hierarchical construction to bioinspired materials, Nano Today 14 (2017) 16–41.
[20] P. Brocos, N. Diaz-Vergara, X. Banquy, S. Pérez-Casas, M. Costas, A. Pineiro, Similarities and differences between cyclodextrin- sodium dodecyl sulfate host- guest complexes of different stoichiometries: molecular dynamics simulations at several temperatures, J. Phys. Chem. B 114 (39) (2010) 12455–12467.
[21] A.J. Valente, O. Söderman, The formation of host–guest complexes between surfactants and cyclodextrins, Adv. Colloid Interface Sci. 205 (2014) 156–176.
[22] T. Narayanan, O. Konovalov, Synchrotron scattering methods for nanomaterials and soft matter research, Materials 13 (3) (2020) 752.
[23] S. Ouhajji, J. Landman, S. Prévost, L. Jiang, A.P. Philipse, A.V. Petukhov, In situ observation of self-assembly of sugars and surfactants from nanometres to microns, Soft Matter 13 (13) (2017) 2421–2425, https://doi.org/10.1039/C7SM00109F, http://xlink.rsc.org/?DOI=C7SM00109F.
[24] J. Landman, S. Ouhajji, S. Prévost, T. Narayanan, J. Groenewold, A.P. Philipse, W.K. Kegel, A.V. Petukhov, Inward growth by nucleation: multiscale self-assembly of ordered membranes, Sci. Adv. 4 (6) (2018) eaat1817, https://doi.org/10.1126/sciadv.aat1817, http://advances.sciencemag.org/lookup/doi/10.1126/sciadv.aat1817.
[25] L. d, S.S. Araújo, L. Watson, D.A. Traore, G. Lazzara, L. Chiappisi, Hierarchical assembly of pH-responsive surfactant–cyclodextrin complexes, Soft Matter 18 (35) (2022) 6529–6537.
[26] L. dos Santos Silva Araújo, G. Lazzara, L. Chiappisi, Thermoresponsive behavior of cyclodextrin inclusion complexes with weakly anionic alkyl ethoxy carboxylates, Soft Matter 19 (8) (2023) 1523–1530, https://doi.org/10.1039/d2sm01621d.
[27] M. Bilal, C. De Brauer, P. Claudy, P. Germain, J. Létoffé, β-cyclodextrin hydration: a calorimetric and gravimetric study, Thermochim. Acta 249 (1995) 63–73.
[28] T. Narayanan, M. Sztucki, T. Zinn, J. Kieffer, A. Homs-Puron, J. Gorini, P. Van Vaerenbergh, P. Boesecke, Performance of the time-resolved ultra-small-angle x-ray scattering beamline with the extremely brilliant source, J. Appl. Crystallogr. 55 (1) (2022) 98–111.
[29] M. Sztucki, Saxsutilities2: a graphical user interface for processing and analysis of small-angle x-ray scattering data (zenodo), https://doi.org/10.5281/zenodo.5825707, Sep. 2021.
[30] A.V. Petoukhov, J. Landman, T. Komarova, Kinetics of multiscale self-organisation via a pressure jump, https://doi.org/10.15151/ESRF-ES-542848883, 2024.
[31] B. Huberman, D. Lublin, S. Doniach, A theory of melting in liquid crystals, Solid State Commun. 17 (4) (1975) 485–488, https://doi.org/10.1016/0038-1098(75)90483-4, https://www.sciencedirect.com/science/article/pii/0038109875904834.
[32] P.-c. Chen, J.S. Hub, Validating solution ensembles from molecular dynamics simulation by wide-angle x-ray scattering data, Biophys. J. 107 (2) (2014) 435–447.
[33] C.J. Knight, J.S. Hub, Waxsis: a web server for the calculation of saxs/waxs curves based on explicit-solvent molecular dynamics, Nucleic Acids Res. 43 (W1) (2015) W225–W230.
[34] S. Datz, B. Illes, D. Gößl, C.v. Schirnding, H. Engelke, T. Bein, Biocompatible crosslinked β-cyclodextrin nanoparticles as multifunctional carriers for cellular delivery, Nanoscale 10 (34) (2018) 16284–16292.
[35] Z.S. Abbas, G.M. Sulaiman, M.S. Jabir, S.A. Mohammed, R.A. Khan, H.A. Mohammed, A. Al-Subaiyel, Galangin/β-cyclodextrin inclusion complex as a drug-delivery system for improved solubility and biocompatibility in breast cancer treatment, Molecules 27 (14) (2022) 4521.
[36] I. Livsey, Neutron scattering from concentric cylinders. Intraparticle interference function and radius of gyration, J. Chem. Soc. Faraday Trans. II 83 (8) (1987) 1445, https://doi.org/10.1039/f29878301445, http://xlink.rsc.org/?DOI=f29878301445.
[37] E. Paineau, M.-E.M. Krapf, M.-S. Amara, N.V. Matskova, I. Dozov, S. Rouzière, A. Thill, P. Launois, P. Davidson, Highly-dilute suspensions of imogolite nanotubes, Nat. Commun. 7 (2016) 10271, https://doi.org/10.1038/ncomms10271.
[38] O. Kratky, G. Porod, Diffuse small-angle scattering of x-rays in colloid systems, J. Colloid Sci. 4 (1) (1949) 35–70.
[39] K.K. Konstantin Koschke, Hans Jörg Limbach, D. Donadio, Freezing point depression in model Lennard-Jones solutions, Mol. Phys. 113 (17–18) (2015) 2725–2734, https://doi.org/10.1080/00268976.2015.1029029.
[40] J.F. Nagle, Experimentally determined tilt and bending moduli of single-component lipid bilayers, Chem. Phys. Lipids 205 (2017) 18–24, https://doi.org/10.1016/j.chemphyslip.2017.04.006.
[41] J. Eid, H. Razmazma, A. Jraij, A. Ebrahimi, L. Monticelli, On calculating the bending modulus of lipid bilayer membranes from buckling simulations, J. Phys. Chem. B 124 (29) (2020) 6299–6311, https://doi.org/10.1021/acs.jpcb.0c04253.
[42] H. Wang, W. Xiong, Revealing the molecular physics of lattice self-assembly by vibrational hyperspectral imaging, Langmuir 38 (10) (2022) 3017–3031, https://doi.org/10.1021/acs.langmuir.1c03313.
[43] B. Bhat, S. Pahari, J.S.-I. Kwon, M.E.S. Akbulut, Rheological dynamics and structural characteristics of supramolecular assemblies of β-cyclodextrin and sulfonic surfactants, Soft Matter 19 (12) (2023) 2231–2240, https://doi.org/10.1039/d3sm00132f.
[44] W. Helfrich, R.M. Servuss, Undulations, steric interaction and cohesion of fluid membranes, Nuovo Cimento D 3 (1) (1984) 137–151, https://doi.org/10.1007/BF02452208.
[45] R. Dimova, Recent developments in the field of bending rigidity measurements on membranes, Adv. Colloid Interface Sci. 208 (2014) 225–234.
[46] P.D. Ross, M.V. Rekharsky, Thermodynamics of hydrogen bond and hydrophobic interactions in cyclodextrin complexes, Biophys. J. 71 (4) (1996) 2144–2154.
[47] C. Tanford, The Hydrophobic Effect: Formation of Micelles and Biological Membranes, 2d ed, J. Wiley, 1980.
[48] D.E. Discher, A. Eisenberg, Polymer vesicles, Science 297 (5583) (2002) 967–973.
[49] M.S. Nikolic, C. Olsson, A. Salcher, A. Kornowski, A. Rank, R. Schubert, A. Frömsdorf, H. Weller, S. Förster, Micelle and vesicle formation of amphiphilic nanoparticles, Angew. Chem. 121 (15) (2009) 2790–2792.
[50] J. Hernández-Muñoz, F. Bresme, P. Tarazona, E. Chacón, Bending modulus of lipid membranes from density correlation functions, J. Chem. Theory Comput. 18 (5) (2022) 3151–3163, https://doi.org/10.1021/acs.jctc.2c00099.
[51] L. Jiang, J.W.J. de Folter, J. Huang, A.P. Philipse, W.K. Kegel, A.V. Petukhov, Helical colloidal sphere structures through thermo-reversible co-assembly with molecular microtubes, Angew. Chem., Int. Ed. Engl. 52 (12) (2013) 3364–3368, https://doi.org/10.1002/anie.201209767, http://www.ncbi.nlm.nih.gov/pubmed/23441056, http://doi.wiley.com/10.1002/anie.201209767.
[52] J.W.J. de Folter, P. Liu, L. Jiang, A. Kuijk, H.E. Bakker, A. Imhof, A. van Blaaderen, J. Huang, W.K. Kegel, A.P. Philipse, A.V. Petukhov, Self-organization of anisotropic and binary colloids in thermo-switchable 1d microconfinement, Part. Part. Syst. Charact. 32 (3) (2014) 313–320, https://doi.org/10.1002/ppsc.201400132.
[53] H.W. Kroto, J.R. Heath, S.C. O'Brien, R.F. Curl, R.E. Smalley, C60: buckminsterfullerene, Nature 318 (11) (1985) 162.
[54] M. Kogiso, Self-assembled peptide fibers from valylvaline bola-amphiphiles by a parallel β-sheet network, Biochim. Biophys. Acta, Gen. Subj. 1475 (3) (2000) 346–352, https://doi.org/10.1016/S0304-4165(00)00088-X, http://linkinghub.elsevier.com/retrieve/pii/S030441650000088X.
[55] A.J. Page, F. Ding, S. Irle, K. Morokuma, Insights into carbon nanotube and graphene formation mechanisms from molecular simulations: a review, Rep. Prog. Phys. 78 (2015) 036501, https://doi.org/10.1088/0034-4885/78/3/036501.
[56] F. Caimi, G. Zanchetta, Twisted structures in natural and bioinspired molecules: self-assembly and propagation of chirality across multiple length scales, ACS Omega 8 (20) (2023) 17350–17361, https://doi.org/10.1021/acsomega.3c01822.
[57] H. Qiu, Z.M. Hudson, M.A. Winnik, I. Manners, Multidimensional hierarchical self-assembly of amphiphilic cylindrical block comicelles, Science 347 (6228) (2015) 1329–1332, https://doi.org/10.1126/science.1261816.
[58] J.-P. Douliez, B. Houinsou-houssou, A.-L. Fameau, B. Novales, C. Gaillard, L. Navailles, F. Nallet, 12-Hydroxystearic acid lipid tubes under various experimental conditions, J. Colloid Interface Sci. 341 (1) (2010) 38–47, https://doi.org/10.1016/j.jcis.2009.09.034, http://www.ncbi.nlm.nih.gov/pubmed/19846108, https://doi.org/10.1016/j.jcis.2009.09.061, http://www.ncbi.nlm.nih.gov/pubmed/19879592.
[59] R. Takahashi, H. Kawauchi, N. Kameta, J.H. Lee, S. Fujii, T. Shimizu, K. Sakurai, Observing the kinetic pathway of nanotube formation from bolaamphiphiles by time-resolved small-angle x-ray scattering, J. Phys. Chem. B 123 (19) (2019) 4340–4345.
[60] C. Song, Y. Li, Y. Luan, S. Liu, Z. Guo, F. Xu, Study on the strengthening and toughening design of the interlayer interface of go-based bionic nacre composites and its optimization mechanisms, Compos. Sci. Technol. 223 (2022) 109423, https://doi.org/10.1016/j.compscitech.2022.109423, https://www.sciencedirect.com/science/article/pii/S0266353822001658.